J Mater Sci: Mater Electron (2014) 25:4992–4999
DOI 10.1007/s10854-014-2262-y

Effect of annealing time on the structural, optical and electrical characteristics of DC sputtered ITO thin films

S. D. Senol · A. Senol · O. Ozturk · M. Erdem

Received: 7 July 2014 / Accepted: 16 August 2014 / Published online: 23 August 2014

Abstract Using an Indium tin oxide (ITO) ceramic target (In_2O_3:SnO_2, 90:10 wt%), ITO thin films were deposited by conventional direct current magnetron sputtering technique onto glass substrates at room temperature. The obtained ITO films were annealed at 400 °C for different annealing times (1, 2, 5, 7, and 9 h). The effect of annealing time on their structural, optical and electrical properties was investigated by X-ray diffraction (XRD), scanning electron microscopy (SEM), atomic force microcopy (AFM), ultra violet–visible (UV–Vis) spectrometer, and temperature dependence Hall measurements. XRD data of obtained ITO films reveal that the films were polycrystalline with cubic structure and exhibit (222), (400) and (440) crystallographic planes of In_2O_3. AFM and Scanning Electron Microscopy SEM have been used to probe the surface roughness and the morphology of the films. The refractive index (n), thickness and porosity (%) of the films were evaluated from transmittance spectra obtained in the range 350–700 nm by UV–Vis. The optical band gap of ITO film was found to be varying from 3.35 to 3.47 eV with the annealing time. The annealing time dependence of resistivity, carrier concentration, carrier mobility, sheet resistance, and figure of merit values of the films at room temperature were discussed. The carrier concentration of the films increased from 1.21×10^{20} to 1.90×10^{20} cm^{-3}, the Hall mobility increased from 11.38 to 18 cm^2 V^{-1} s^{-1} and electrical resistivity decreased from 3.97×10^{-3} to 2.13×10^{-3} Ω cm with the increase of annealing time from 1 to 9 h. Additionally, the temperature dependence of the carrier concentration, and carrier mobility for the as-deposited and 400 °C annealed ITO films for 2 and 9 h were analysed in the temperature range of 80–350 K.

1 Introduction

Indium tin oxide (ITO) films have high optical transmittance in the visible wave length region because of being a wide band gap semiconductor (e.g. 3.5 eV), low resistivity due to a high carrier concentration (10^{20}–10^{21} cm^{-3}), excellent adhesion to substrates, chemical stability and photochemical properties [1]. Owing to these properties, ITO films has been extensively used as a transparent electrode for potential technological and industrial applications in optoelectronic devices such as solar cells [2], liquid crystal displays (LCD's) [3], and light-emitting diodes (LEDs) [4, 5]. Various deposition techniques such as spray pyrolysis [6], sol–gel process [7], chemical vapor deposition [8], thermal evaporation [9], electron beam evaporation [10], pulsed laser deposition [11] and magnetron sputtering [12–14] have been developed to meet both technological and economic demands for preparing high quality ITO thin films. The sputtering technique comes to fore for the deposition of ITO films due to its high deposition rate, large deposition area, low substrate heating, and reproducibility [1].

S. D. Senol (✉)
Department of Chemistry, Abant Izzet Baysal University, 14280 Bolu, Turkey
e-mail: demirozu_s@ibu.edu.tr

A. Senol · O. Ozturk
Department of Physics, Kastamonu University, 37100 Kastamonu, Turkey

M. Erdem
Department of Physics, Abant Izzet Baysal University, 14280 Bolu, Turkey

Heat treatment plays an important role on the structural, electrical and optical properties of ITO films since it can modify structure (structural defects, grain size and shape, etc.) and purity (nature and concentration of impurities, absorbed and adsorbed gases, etc.) of the films. Studying the effect of heat treatment on these properties of ITO films can give valuable information on the processes taking place. It is reported that the optimum annealing temperature is 400 °C for direct current (DC) magnetron sputtered ITO films [14]. Hence, in the present work the annealing temperature is taken as 400 °C and the annealing time is varied to investigate the effect on structural, optical and electrical properties of ITO films prepared by DC sputtering deposited on glass substrate.

2 Experimental

2.1 Preparation of thin film

ITO thin films were deposited on sodalime glasses using NSC–3000 DC magnetron sputtering system. The composition of the ITO target (a 4 mm in thickness and 50 mm in diameter) used in this study was 90 wt% In_2O_3 and 10 wt% SnO_2 with a purity of 99.99 %. The glass substrates were cleaned in acetone bath by an ultrasonic cleaner, degreased in a dilute detergent solution rinsed in de-ionized water, and subsequently dried in a flowing nitrogen gas before deposition process. The distance between the target and the substrates was 60 mm. The vacuum chamber was evacuated down to pressure 10^{-6} Torr prior to deposition. The DC power during the film deposition was 100 W. The sputtering process is performed for 15 min at room temperature by using 99.999 % pure Ar gas (30 sscm). In order to determine the annealing effect on the structural, electro-optical behaviour of the films, the obtained films were annealed at 400 °C for different times (1, 2, 5, 7 and 9 h) and then cooled down to room temperature.

2.2 Characterization of thin film

The phase composition of ITO thin films were performed using Rigaku Multiflex X-ray diffraction (XRD) instrument at room temperature, with monochromated Cu Kα ($\lambda = 1.5418$ Å), in the scan range of 2θ between 10° and 60° with a scan speed of 3°/min and a step increment of 0.02. Measurements were taken under beam-acceleration conditions of 38 kV/28 mA. The optical transmission and refraction spectra of the films were measured by a JASCO 430 UV–Vis spectrophotometer by in the spectral range of 400–700 nm with the unpolarized light at normal incidence. Optical parameters namely refractive index, thickness, porosity and optical band gap energy were calculated using these transmission spectra of the films. The surface morphology of the thin film samples was obtained using an atomic force microscopy (AFM) instrument (Nanomagnetic Instrument) in contact mode. The surface morphologies and cross-section were observed by scanning electron microscopy (SEM) (JEOL 6390-LV). To measure electrical properties, the samples were cut into the square size about 1 × 1 cm^2 and the four corners of the films were soldered by silver blobs for the ohmic contacts. Applying a constant current of 5 mA and magnetic field of 0.55 T, the resistivity, carrier density, mobility of the films were measured by using temperature-dependent van der Pauw method with Ecopia HMS-5000 Hall-effect measurement system in the temperature range of 80–350 K.

3 Result and discussion

3.1 Structural properties

Figure 1 shows XRD patterns of ITO films for as-deposited and annealed at 400 °C for different times namely, 1, 2, 5, 7 and 9 h. It is seen from XRD patterns that all deposited ITO thin films including the as-deposited one are crystalline and have (222), (400) and (440) preferred orientations in <111>, <100> and <110> directions, respectively. All the patterns match with the cubic bixbyite structure of In_2O_3 reference peaks (ICDD 06-0416). None of the characteristic peaks of Sn, SnO and SnO_2 appear in XRD patterns, which means that all tin atoms were probably doped substitutionally into the In_2O_3. The intensity of (222) peak does not change considerably up to 9 h of annealing at which it reaches a maximum while the intensity of (400) peak reaches a maximum for 5 h. Above 5 h, the (400) peak decreases and disappears at 9 h. The (440) peak intensity becomes evident with annealing and no remarkable variation of intensity is observed with increasing annealing time. The effect of annealing time causes an interplay of crystal growth among <111> and <100> directions. The increase in the annealing time causes more oxygen outdiffusion from the structure meaning increased oxygen vacancies. Since the structural oxygen vacancies are located along the four <111> axes of ITO unit cell [15], the maximum crystallization in (222) direction seen in XRD peak for 9 h of annealing might be related to the increase in oxygen vacancies. The intensity ratio of (222) to (400) peaks, which is known as the crystal quality parameter, is calculated for our films and the results are tabulated in Table 1. As you can see from this table, the highest value (I_{222}/I_{400}) is obtained for the film annealed for 9 h, which shows preferred crystal growth towards (222) direction. In addition to preferred orientation analysis, the crystallite size of obtained ITO films can be

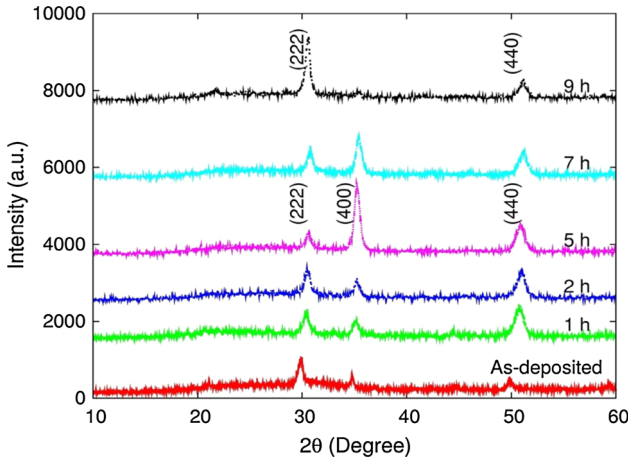

Fig. 1 XRD patterns for an as-deposited and annealed ITO films at 400 °C for different annealing times

determined by the full width at half maximum (FWHM) of the XRD peaks, using the Scherrer formula [16]

$$D = \frac{k\lambda}{B\cos\theta} \quad (1)$$

where k is the shape factor possessing a numerical value of 0.9, λ is the wavelength of the used XRD data, B is the FWHM of the measured peak in radians, θ is the Bragg's angle. From Table 1, the crystallite size for annealed films tends to increase by increasing annealing time from 1 to 9 h, showing better cystallinity with increasing annealing time. This result is due to the effect of crystallization annealing duration on the growth morphology of the crystals. Furthermore, the calculated lattice constants (from strongest peaks of XRD data) and plane distances of films are listed in Table 1. The plane distances associated with (400) orientation decrease with increasing annealing time which shows that increasing annealing time allows more Sn^{+4} ions replace In^{+3} ions in the lattice. Since the ionic radius of Sn^{+4} (69 pm) is less than that of In^{+3} (80 pm), the decrease of plane distances can be explained by substitution of In^{+3} ions by Sn^{+4} ions.

The surface structures of the produced ITO films were analyzed via AFM. Figure 2a–b show 5 × 5 μm scanned AFM images of the as-deposited and 9 h annealed films, respectively. From these images, the root-mean-square surface roughness (R_{rms}) values of the films are found as 5.47 and 4.88 nm for the as-deposited and 9 h annealed films, respectively.

Figure 3 depicts the surface morphologies of (a) as-deposited (b) 5 h annealed and (c) 9 h annealed films. From the figures one can see that as-deposited film is not homogeneous and it has large voids (pores). As the film is annealed, more homogeneous granular structure is obtained due to crystallinity and the porosity decreases. With increasing annealing time, the porosity further decreases and is minimum for 9 h of annealing. This result may be explained by the increase of grain sizes as seen in Table 1. The grains grow into the voids in the sample so the porosity decreases. Moreover, the cross-section SEM image of obtained ITO thin film annealed at 400 °C for 9 h is depicted in Fig. 3d. The thickness of the film is observed to be about 600 nm. Before SEM analysis, the sample was cut near the center in order to get rid of the edge effect.

3.2 Optical properties

One of the essential properties in evaluating the optical properties of ITO thin films in the visible region is transmittance spectra. Optical band gap energy, refraction index, thickness, and porosity can be calculated using the transmittance spectra. In Fig. 4, the measurements of the intensity of the transmitted light from the produced ITO films as a function of wavelength is shown. It is seen from this figure, that owing to the onset of fundamental absorbtion, the optical transmission declines very sharply near the UV region and the onset of optical transmittance edge shifts towards lower wavelengths with increasing annealing time. Thus, widening of the high transmittance region due to this shifting is observed which enables us to use wider range of wavelength in optical applications of ITO thin films. The as-deposited film has the lowest transmittance in the visible region while the films annealed for 2, 5, and 9 h have transmittance over 80 % in the 400–700 nm region. The optical transparency and its

Table 1 The ratio peak intensity of (222) and (400) (I_{222}/I_{400}), texture, plane distances and grain sizes of ITO films for as-deposited and annealed at 400 °C for different times

Sample name	I_{222}/I_{400}	Film texture	(222) Plane distance (Å)	(400) Plane distance (Å)	Lattice constant (Å)	Grain size from XRD (nm)
As-deposited	1.923	<111>	2.978	2.577	10.316	11.08
1 h	1.387	<111>	2.930	2.547	10.149	8.87
2 h	1.493	<111>	2.936	2.544	10.171	9.84
5 h	0.310	<100>	2.917	2.544	10.176	9.12
7 h	0.730	<111>	2.904	2.531	10.124	11.7
9 h	6.670	<111>	2.917	2.529	10.105	14.68

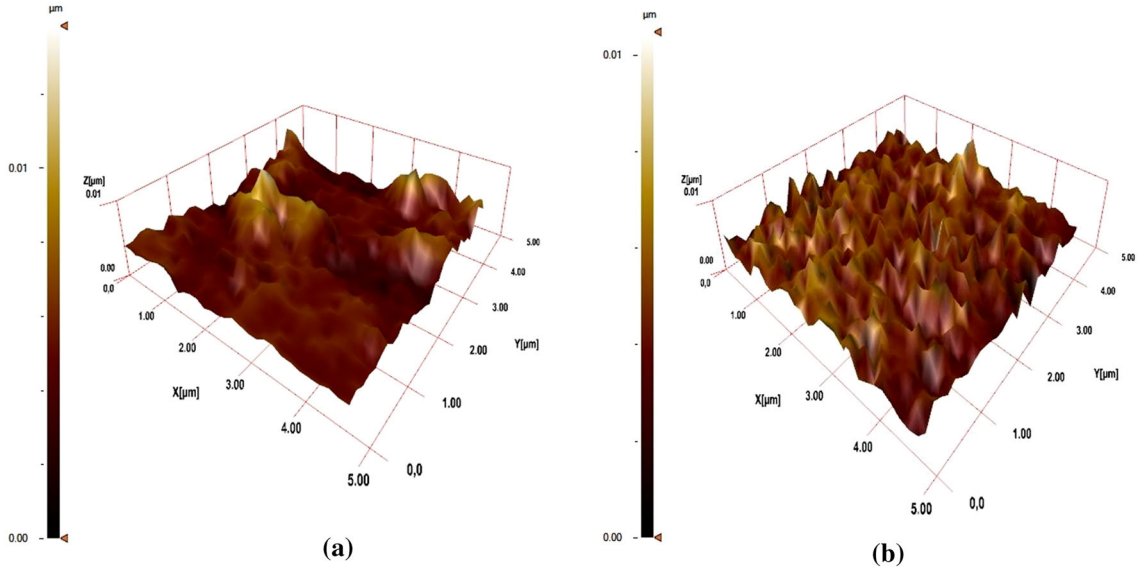

Fig. 2 AFM surface images of ITO thin films **a** as-deposited and **b** annealed at 400 °C for 9 h

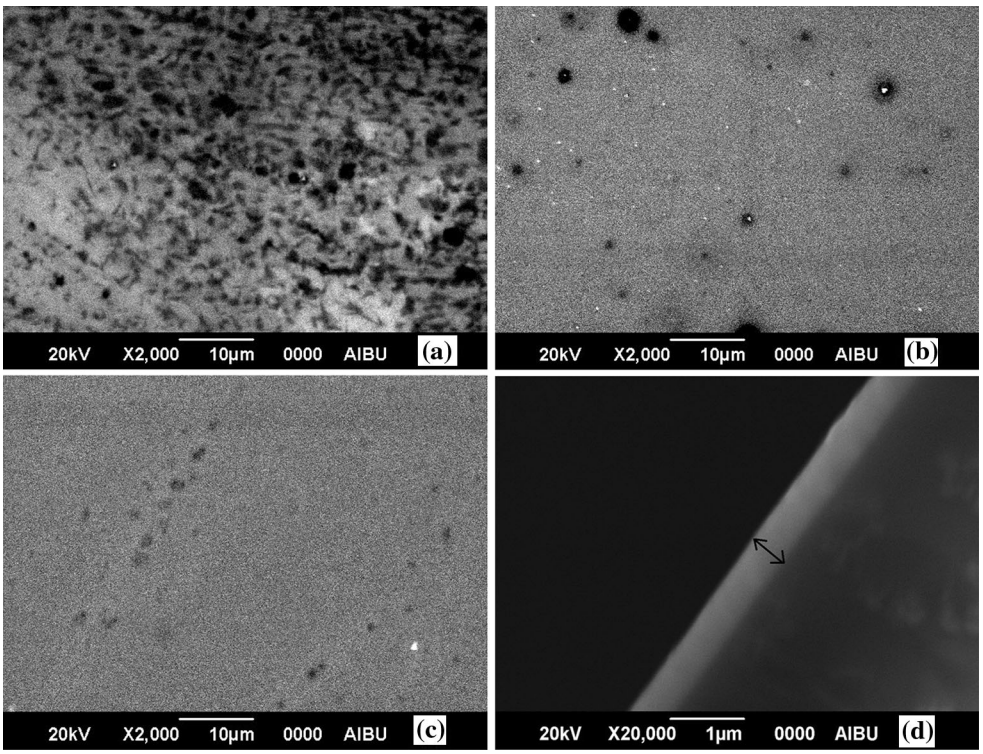

Fig. 3 Surface SEM images of **a** as-deposited, **b** 5 h annealed, **c** 9 h annealed films and **d** cross-section of 9 h annealed film (double-sided arrow shows the thickness of the film)

variation as a function of wavelength does not significantly change with the annealing time beyond 2 h. High transmittance in polycrystalline thin films is associated with structural homogeneity, less scattering effect due to decrease of roughness and better crystallinity. Among the high performing three thin films (2, 5, 9 h) the 9 h annealed film has slightly less transmittance above 450 nm which is due to the free carrier absorbtion. For the 9 h annealed film, the free carrier concentration is the highest (Table 3) causing an increase in the scattering probability of incident

Table 2 The refractive index, thickness, porosity and the optical band gap (E_g) values for as-deposited and annealed films

Sample name	Refractive index	Thickness (nm)	Porosity (%)	Optical band gap (eV)
As-deposited	1.77	638	37.45	3.35
1 h	1.82	673	32.18	3.40
2 h	1.83	675	31.12	3.43
5 h	1.84	667	30.04	3.45
9 h	1.84	674	30.04	3.47

light. Moreover, the transmittance values for all samples converge to about 88 % at 700 nm.

The Swanepoel method used in this work to determine refractive index of ITO films in spectral range of 300–700 nm is based on the analysis of the transmittance spectrum of a weakly absorbing film deposited on a non-absorbing substrate [17]. The refractive index (n) can be calculated from following equations [18].

$$n = [N + (N^2 - s^2)^{1/2}]^{1/2} \quad (2)$$

where

$N = \frac{2s(T_M - T_m)}{T_M T_m} + (s^2 + 1)/2$, s is the refractive index of the glass substrate, T_M and T_m are the maximum and the minimum transmittance of the envelope of interference, respectively. For any λ, T_M has a correspondent value T_m. Also, we can evaluate the thickness of the films from their transmittance spectra by [18].

$$d = \lambda_1\lambda_2/2\ (\lambda_1 n_2 - \lambda_2 n_1), \quad (3)$$

here n_1 and n_2 are the refractive indices at two close maxima (or minima) at λ_1 and λ_2. Further more, porosity values of some ITO-samples were calculated by using following equation [19]:

$$Porosity = \left(1 - \frac{n^2 - 1}{n_d^2 - 1}\right) \times 100\,\% \quad (4)$$

where n_d is the refractive index of pore-free ITO = 2.1 [20] and n is the refractive index of the porous thin films.

The calculated values of refractive index, thickness and porosity of ITO films as-deposited and with different annealing times of films at 400 °C are summarized in Table 2. In the calculation, the value of λ was taken in the range 580–600 nm. The calculated refractive index values are in good agreement with the values given in the literature [21–23]. In Table 2, the porosities of the films decrease from 37.45 to 30.04 % with annealing time which is in good agreement with the SEM images given in Fig. 3. The SEM image in Fig. 3d gave a thickness value of about 600 nm which is comparable to the calculated thickness values of all the samples from Fig. 4.

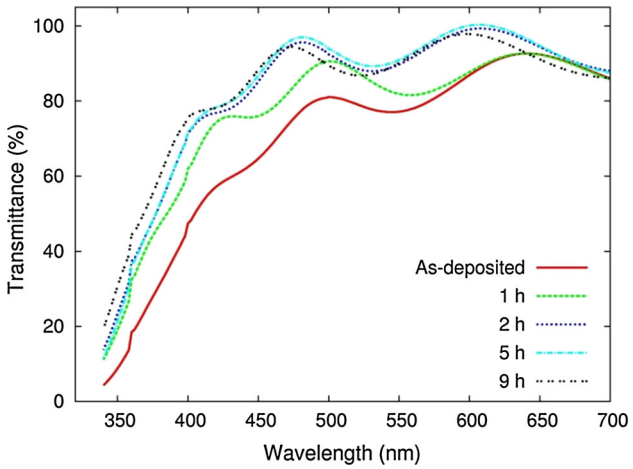

Fig. 4 Transmittance spectra of as-deposited and annealed ITO films in visible region

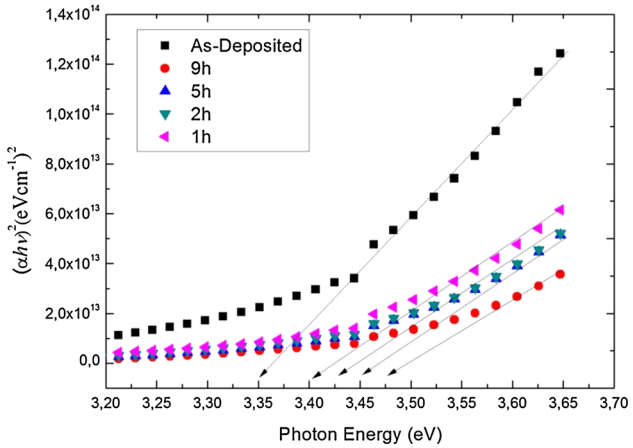

Fig. 5 The variation of $(\alpha h\nu)^2$ with the photon energy of ITO thin films

The relation between the optical band gap (E_g) and absorption coefficient (α) obtained from measurement of the absorption spectrum of ITO films can be determined by following:

$$\alpha h\nu = A(h\nu - E_g)^m \quad (5)$$

where α is obtained from measurement of the absorption spectrum, h is Planck's constant, A denotes a parameter proportional to the transition probability, $h\nu$ is the energy of the photon and m is 1/2 for allowed direct, 2 for allowed indirect, 3/2 for forbidden direct, 3 for forbidden indirect optical transitions [24]. Assuming directly allowed transition, the Tauc plot of $(\alpha h\upsilon)^2$ versus photon energy ($h\upsilon$) for the all studied ITO films were presented in Fig. 5. The band gap energy was evaluated by extrapolating the linear part of the Tauc plot curves to intercept the energy axis (at

Table 3 The electrical properties and figure of merit values of the films

Sample name	Carrier concentration (cm^{-3})	Hall mobility ($cm^2/V\ s$)	Resistivity (Ωcm)	Sheet resistance (Ω/square)	Mean free path (nm)	Figure of merit (Ω^{-1})
As-deposited	0.99×10^{20}	15.77	3.97×10^{-3}	81.66	1.49	9.15×10^{-4}
1 h	1.21×10^{20}	11.38	4.55×10^{-3}	65.81	1.15	2.06×10^{-3}
2 h	1.26×10^{20}	12.37	4.02×10^{-3}	61.71	1.26	5.50×10^{-3}
5 h	1.27×10^{20}	15.36	3.20×10^{-3}	47.73	1.57	1.07×10^{-2}
9 h	1.90×10^{20}	15.48	2.13×10^{-3}	30.17	1.81	1.18×10^{-2}

$\alpha = 0$) and the results are listed in Table 2. The values of optical band gap were found to increase from 3.35 to 3.47 eV with annealing time that is typical for a wide-band gap semiconductor and is in good agreement with the reported data in the literature [25, 26]. The widening of the optical band gap with annealing time may be related to the partial filling of the conduction band by the free carriers due to the blocking of the lower states which is known as the Burstein–Moss effect [27]. This phenomenon is confirmed by the increase of carrier concentration with the annealing time for our samples as given in Table 3.

3.3 Electrical properties

The effects of annealing time on electrical properties of the ITO films were performed by temperature-dependent van der Pauw Hall measurements in the temperature range 80–350 K. The carrier concentration, Hall mobility, resistivity, sheet resistance, mean free path and figure of merit values at room temperature are shown in Table 3.

The carrier concentration increases with annealing time and especially the increase for 9 h is significant. As confirmed by XRD results, increasing the annealing time casuses more Sn^{+4} ions to diffuse into the In_2O_3 lattice and substitute In^{+3} from grain boundaries and interstitial lattice locations. Since Sn^{+4} has higher valency than In^{+3}, it behaves as donor in ITO films [28]. Morever, the oxygen vacancies increase with annealing time due to oxygen outdiffusion, since oxygen acts as an acceptor, the lost of oxygen causes an increase in the free electron concentration.

In polycrystalline solids, the transport electrical properties, i.e. Hall mobility, conductivity-the inverse of resistivity-, and mean free path are governed mainly by the scattering of charge carries. The main sources of the scattering are crystal defects, impurities (especially the ionized impurities), phonons and grain boundaries. When the effect of scattering mechanism is reduced, the Hall mobility, conductivity, and the mean free path are expected to increase. The mean free path values of the free carriers as a function of carrier concentration and Hall mobility for these films are calculated by the following relation [29]

$$l = \frac{h}{2e}\left(\frac{3n}{\pi}\right)^{1/3} \mu_H \tag{6}$$

where n is the carrier concentration and μ_H is the Hall mobility. The calculated mean free path values are in the range of 1.49 and 1.81 nm.

A detailed examination of Table 3 reveals that, a decrease in Hall mobility, conductivity and mean free path values are observed when the as-deposited film is annealed for 1 h, but they increase with annealing time. This behaviour is coherent to the change in grain sizes given in Table 1. The results show that, the grain boundary scattering of the charge carriers is more dominant in the obtained films. Because grain boundaries are the main sites for precipitates and ionized impurities, the increase of grain size hence decrease of the electron scattering at the grain boundaries results in the increase of electrical properties [30–32].

The conductivity in the polycrystalline samples increases when there is better connectivity among the grains. Conversely, the voids or pores in the sample lead to loss of intergranular connectivity hence increase the resistivity. From the SEM images and the calculated porosities using optical properties of the films, the decrease of porosity with longer annealing time is confirmed. So another factor causing the decrease of resistivity with annealing time is the decrease of porosity values with time.

The sheet resistance of the samples was calculated by using the vander Pauw equation [33, 34]

$$R_s = \frac{\pi R_A}{\ln 2} \tag{7}$$

$$R_A = \frac{V_{43}}{I_{12}}$$

where I_{12} is caused to flow along one edge of the sample and V_{43} is the voltage across the opposite edge. As you can see from Table 3, the sheet resistance decreases as the annealing time increased. The decrease in sheet resistance

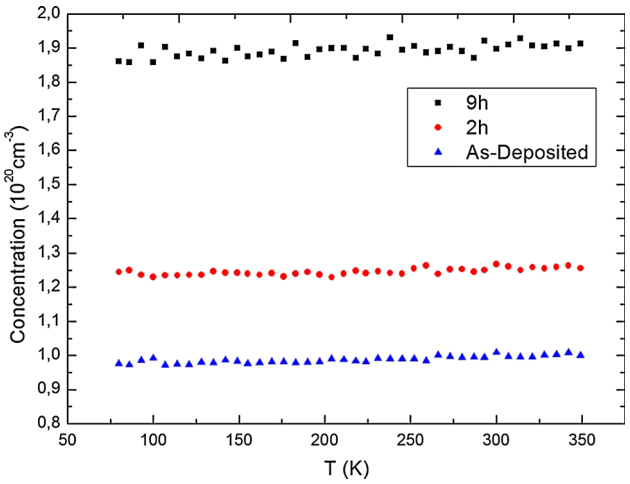

Fig. 6 Temperature-dependent carrier concentration of ITO films for as-deposited and annealed at 400 °C for 2 and 9 h

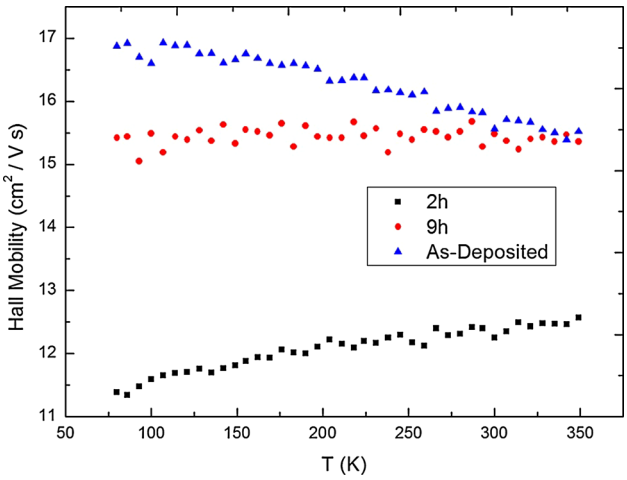

Fig. 7 Temperature-dependent behaviour of Hall mobility of ITO films for as-deposited and annealed at 400 °C for 2 h

with increasing annealing time could be due to the improved crystalline nature of the films.

For the technological applications of ITO thin films, not only high transparency in the visible region, but also low resistivity is essential. The quality of the thin films in this respect can be judged using the figure of merit (ϕ). The figure of merit of the films can be calculated using the values of sheet resistance (R_S) and optical transmittance at a specified wavelength by Haacke's relation [35]

$$\phi = T^{10}/R_S$$

The figure of merit values are calculated with the transmittance of the films at 550 nm and are listed in Table 3. The quality of the films is seen to increase with annealing time and the highest figure of merit ($1.18 \times 10^{-2}\ \Omega^{-1}$) is obtained for 9 h annealed film.

Figures 6 and 7 show the temperature dependence of the carrier concentration, Hall mobility for as-deposited, 2 and 9 h annealed films, respectively. No significant change in the carrier concentrations with respect to temperature is observed for all samples. It is well known that mobility is dominated by ionized impurity scattering at lower temperatures, while at higher temperatures, phonon scattering dominates [36]. For the as-deposited film, the mobility increases linearly with decreasing temperature as expected due to the decrease of phonon vibrations. But for the 2 h annealed sample, the mobility decreases linearly with decreasing temperature. At low temperatures, the carrier electrons move slowly so they spend more time when passing an impurity ion. The ion impurity scatterings which have little impact on high energy electrons become dominant causing the mobility to decrease as temperature decreases. In our case, the 2 h annealed film has the smallest grains among the three films, which means increased number of grain boundaries and since the diffusion of tin atoms into the lattice is not completed yet, some tin atoms locate at the grain boundaries forming scattering centers. As a result, the mobility for 2 h annealed film is expected to decrease with decreasing temperature. For the 9 h annealed film however, larger grains are formed and there is more diffusion of tin atoms into the lattice. So, both mechanisms act as to decrease the number of impurity sites. The mobility of the 9 h annealed film is expected to increase with decreasing temperature, but the mobility is almost constant in the measurement range. There seems to be an unclear mechanism which suppresses the increase of mobility at low temperatures.

4 Conclusion

The effect of annealing time on the structural, optical, and electrical properties of DC sputtered ITO thin films is studied. XRD results reveal that more tin atoms diffuse into the lattice structure and the grain sizes increase with increasing annealing time. The surface roughness and porosity decrease and better crystallinity is obtained for longer annealing. The optical measurements show that the 2, 5, and 9 h annealed samples have transmittance values above 80 % in the visible range. The electrical measurements are made by van der Pauw method in the 80–350 K temperature range. At the room temperature, the carrier concentration, and the mobility increase with annealing time. Moreover, the resistivity and sheet resistance decrease with annealing time. The optical band gap increases with annealing time due to Burstein–Moss effect. The figure of merit which is a function of both transmittance and sheet resistance is an important parameter for

technological applications of transparent conducting thin films. Among the best transmitting thin films, the 9 h annealed film has slightly lower transmittance. But it has the highest figure of merit because of its low sheet resistance. The carrier concentrations do not change appreciably in the 80–350 K temperature range. The Hall mobility increases for the as-deposited film, it decreases for 2 h annealed film and does not vary with decreasing temperature in the same range.

Acknowledgments A.S. would like to thank Abant Izzet Baysal University Department of Physics where this study was carried out, for their hospitality. Authors would like to thank A. Varilci and C. Terzioglu for valuable suggestions and comments.

References

1. R.B.H. Tahar, T. Ban, Y. Ohya, Y. Takahashi, J. Appl. Phys. **83**, 2139 (1998)
2. K.L. Chopra, S. Mayor, D.K. Pandya, Thin Solid Films **102**, 1 (1983)
3. T. Minami, Thin Solid Films **516**, 5822 (2008)
4. H. Kim, A. Dique, J.S. Horwitz, D.B. Chrisey, Appl. Phys. Lett. **74**, 3444 (1999)
5. H. Liu, V. Avrutin, N. Izyumskaya, U. Ozgur, H. Morkoç, Superlattices Microstruct. **48**, 458 (2010)
6. S. Major, K.L. Chopra, Sol. Energy Mater. **17**, 319 (1988)
7. Y. Djaoued, V.H. Phong, S. Badilescu, P.V. Ashrit, F.E. Girouard, V.V. Truong, Thin Solid Films **293**, 108 (1997)
8. J. Vetrone, Y.W. Chung, J. Vac. Sci. Technol. **A9**, 3041 (1991)
9. F. Zhu, C.H.A. Huan, K. Zhang, A.T.S. Wee, Thin Solid Films **359**, 244 (2000)
10. M. Quaas, C. Eggs, M.L. Ma, H. Wulff, Thin Solid Films **322**, 277 (1998)
11. J.P. Zheng, H.S. Kwok, Appl. Phys. Lett. **63**, 1 (1993)
12. S. Ray, R. Banerjee, N. Basu, A.K. Batabyal, A.K. Barua, J. Appl. Phys. **54**, 3497 (1983)
13. Y. Hu, X. Diao, C. Wang, W. Hao, T. Wang, Vacuum **75**, 183 (2004)
14. M. Gulen, G. Yildirim, S. Bal, A. Varilci, I. Belenli, M. Oz, J. Matter. Sci Mater. Electron. **24**, 467 (2013)
15. N. Nadaud, N. Lequeux et al., J. Solid State Chem. **135**, 140 (1998)
16. R. Jenkins, J.L. deVries, *Worked Examples in X-ray Analysis*, 2nd ed. edn. (Philips Technical Library, Macmillan, 1978)
17. J.C. Manifacier, J. Gasiot, J.P. Fillard, J. Phys. E **9**, 1002 (1976)
18. H.N. Cui, V. Teixeria, A. Monteria, Vacuum **67**, 589 (2002)
19. B.E. Yoldas, P.W. Partlow, Thin Solid Films **129**, 1 (1985)
20. W.W. Mobzen, J. Vac. Sci. Technol. **12**, 99 (1975)
21. V. Malathy, S. Sivaranjani, V.S. Vidhya, T. Balasubramanian, J. Joseph Prince, C. Sanjeeviraja, M. Jayachandran, J. Mater. Sci. Mater. Electron **21**, 1299 (2010)
22. A.N.H. Al-Ajit, S.C. Bayliss, Thin Solid Films **305**, 116 (1997)
23. C.H. Lee, C.S. Huang, Mater. Sci. Eng. B **22**, 223 (1994)
24. J.I. Parkove, *Optical Process in Semiconductors* (Dover Publications Inc., New York, 1971)
25. W.F. Wu, B.S. Shiou, S.T. Hsich, Semi Conduct. Sci. Technol **9**, 1242 (1994)
26. C.H.L. Weijtens, P.A.C. Vanloon, Thin Solid Films **196**, 1 (1991)
27. C.G. Granqvist, A. Hultaker, Thin Solid Films **411**, 1 (2002)
28. L. Meng, M.P. Dos Santos, Thin Solid Films **322**, 56 (1998)
29. S. Noguchi, H. Sakata, J. Phys. D Appl. Phys. **13**, 1129 (1980)
30. B. Radha Krishna, T.K. Subramanyam, B. Srinivasulu Naidu, S. Uthanna, Opt. Mater. **15**, 217 (2000)
31. J. Joseph Prince, S. Ramamurthy, B. Subramanian, C. Sanjeeviraja, M. Jayachandran, J. Cryst. Growth **240**, 142 (2002)
32. A.V. Moholkar, S.M. Pawar et al., JTTEE5 **19**, 531 (2010)
33. L.J. van der Pauw, Philips Res. Rep. **13**, 1 (1958)
34. L.J. van der Pauw, Philips Tech. Rev. **20**, 220 (1958)
35. G. Haacke, Ann. Rev. Mater. Sci. **7**, 73 (1977)
36. O. Tuna, Y. Selamet, G. Aygun, L. Ozyuzer, J. Phys. D Appl. Phys. **43**, 055402 (2010)